







## Article

# Resonant Laser Ionization and Fine-Structure Study of Silver in an Ablation Plume

Omorjit Singh Khwairakpam <sup>1,2,†</sup> , Emilio Mariotti <sup>2,\*,†</sup> , Daniele Scarpa <sup>2,†</sup> , Piergiorgio Nicolosi <sup>3,†</sup> , Alen Khanbekyan <sup>1</sup> , Salvatore Ferracane <sup>2</sup>, Alberto Arzenton <sup>1,2</sup>  and Alberto Andrighetto <sup>2</sup>

<sup>1</sup> Dipartimento di Scienze Fisiche, della Terra e dell'Ambiente, University of Siena, Via Roma 56, 53100 Siena, Italy

<sup>2</sup> INFN-LNL, Viale Università 2, Legnaro, 35020 Padova, Italy

<sup>3</sup> CNR Istituto di Fotonica e Nanotecnologie Padova, University of Padova, Via Trasea 7, 35131 Padova, Italy

\* Correspondence: emilio.mariotti@unisi.it

† These authors contributed equally to this work.

**Featured Application:** Doppler-suppressed spectroscopy in a hot environment, such as an ablation plume, is demonstrated.

**Abstract:** We report on a laser photo-ionization study of silver in relation to the Selective Production of Exotic Species (SPES) project at INFN-LNL in the off-line laser laboratory. In this study, two dye lasers and an ablation laser operating at 10 Hz are used alongside a time-of-flight mass spectrometer (TOF-MS). Isotopic separation of the natural, stable isotopes <sup>107</sup>Ag and <sup>109</sup>Ag was clearly observed in the TOF signal. Resonant photo-ionization of silver was achieved with the use of the scheme  $4d^{10}5s^2S_{1/2} \rightarrow 4d^{10}5p^2P_{3/2}^o \rightarrow 4d^{10}6d^2D_{3/2}$  with transition wavelengths of 328.163 nm and 421.402 nm, respectively. Doppler-suppressed spectroscopy of these transition lines was performed in an ablation plume. Doppler broadening with collinear injection of excitation lasers and the effect of the linewidths of the excitation lasers were investigated. The fine-structure splitting of the level  $4d^{10}6d^2D$  ( $J = 5/2$  and  $J = 3/2$ ) was confirmed to be  $186 \pm 2$  pm, corresponding to  $314 \pm 3$  GHz.

**Keywords:** Doppler-suppressed profiles; laser spectroscopy; photo-ionization; silver



**Citation:** Khwairakpam, O.S.; Mariotti, E.; Scarpa, D.; Nicolosi, P.; Khanbekyan, A.; Ferracane, S.; Arzenton, A.; Andrighetto, A. Resonant Laser Ionization and Fine-Structure Study of Silver in an Ablation Plume. *Appl. Sci.* **2023**, *13*, 309. <https://doi.org/10.3390/app13010309>

Academic Editor: Bernhard Wilhelm Roth

Received: 27 November 2022

Revised: 15 December 2022

Accepted: 19 December 2022

Published: 27 December 2022



**Copyright:** © 2022 by the authors. Licensee MDPI, Basel, Switzerland. This article is an open access article distributed under the terms and conditions of the Creative Commons Attribution (CC BY) license (<https://creativecommons.org/licenses/by/4.0/>).

## 1. Introduction

The resonant ionization laser ion source (RILIS) technique has greatly enhanced the production of high-purity isotopic beams in radioactive ion beam (RIB) facilities. This technique is a universally recognized method for highly selective ion production. It is applied by many leading RIB facilities, such as IRIS-PNPI [1], CERN-ISOLDE [2,3], TRIUMF-ISAC [4], GANIL [5], GSI [6], RIKEN [7], JYFL [8], KU Leuven [9], and JG Mainz [10]. Selective Production of Exotic Species (SPES) is a second generation isotope separation on-line (ISOL) facility dedicated to the production of radioactive species and the medical application of radionuclides. The RILIS technique is also employed for RIBs production in SPES @INFN-LNL (Legnaro National Laboratories).

In the SPES project, a uranium carbide (UC<sub>x</sub>) target is bombarded by a proton beam of 200 μA @40 MeV, to produce numerous isotopes. A high purity isotopic beam can be obtained with a combination of element selectivity (provided by the laser ion source) and a mass separator. A set of three Ti-Sa lasers has already been characterized and placed in the SPES laser room for the on-line production of RIBs [11].

In preparation for the SPES project, off-line studies of the laser photo-ionization schemes of several elements were performed. In previous studies, the resonance laser ionizations of germanium [12], tin [13] and aluminum [14] were achieved and isotopic identification was tested in a locally designed time-of-flight mass spectrometer (TOF-MS).

In this article, the off-line laser spectroscopy of silver (Ag,  $Z = 47$ ) is reported. The laser photo-ionization of Ag was successfully achieved during this study. Doppler-suppressed resonance profiles for these transitions are presented. The influence of linewidth of the exciting laser light in a Doppler broadening scenario was also demonstrated. Moreover, the fine structure of the  $4d^{10}6d\ ^2D$  levels was clearly resolved.

## 2. Theory and Motivation

The RILIS relies on a non-thermal process which is based on atomic excitations. Ions of a chosen element are obtained via step-wise resonant energy jumps using, mainly, two or three laser beams tuned to the transition frequencies of the element of interest. The method is chemically very selective as each element has a unique electronic shell structure and energy level scheme. RILIS also has the advantage of high efficiency of the order of tens of percent [15]. The ionization of many elements with relatively high ionization potential (IP), including silver, cannot be achieved optimally with other ion sources, such as surface and plasma ion. The plasma ion source should be able to ionize silver but, for typical on-line experiments using a  $UC_x$  production target, the beam produced will be contaminated. A laser ion source is preferred to produce a high purity beam.

### 2.1. Possible Resonant Schemes of Silver

The  $^{111}\text{Ag}$  isotope is of great interest to the ISOLPHARM project [16] due to its medical properties. It undergoes a  $\beta^-$  decay with a half-life of 7.45 days, with a convenient energy ( $\sim 360$  keV) that corresponds to a medium tissue penetration depth (1.8 mm).

Silver has an ionization potential (IP) of  $61,106.45\text{ cm}^{-1}$  (7.6 eV) [17], which can be efficiently exceeded using RILIS with precise laser wavelengths that correspond to the atomic transitions between the electronic levels. Several known schemes for the photo-ionization of silver have been used in facilities such as IGISOL [18], TRIUMF-ISAC [19] and ISOLDE [20]. A number of electronic levels of silver [17] have been studied and the “radiative” levels which are of interest for our research have been clarified, as shown in Figure 1.

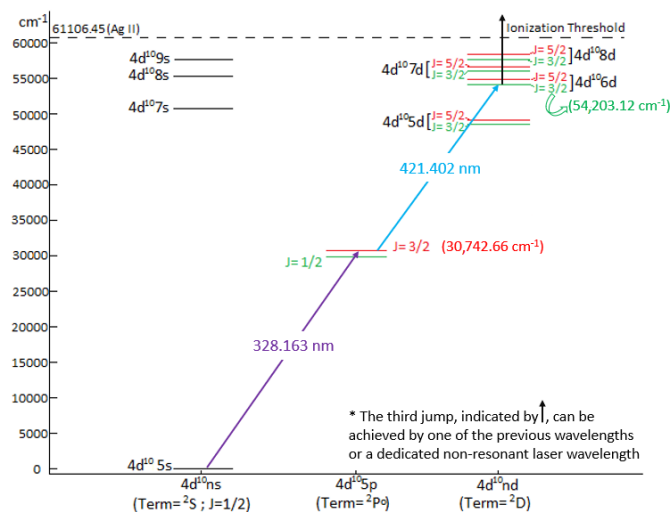


**Figure 1.** Simplified level scheme of Ag and applied excitation path.

Several combinations of these atomic transitions can be used to excite the ground level valence electron beyond the IP. Table 1 presents several selected choices that could provide a pathway for the resonant photo-ionization of Ag. As can be seen from Figure 1, after the two resonant transition steps, the electron has still not crossed the IP. However, from the highest excited level, the electron can be pushed beyond the IP by absorbing a photon from any of the previous excitation steps. Higher ionization efficiencies could be achieved with a third non-resonant laser with sufficient photon energy to cross the gap.

The scheme chosen for this study is the scheme underlined in Table 1:  $4d^{10}5s\ ^2S_{1/2} \rightarrow 4d^{10}5p\ ^2P_{3/2}^o \rightarrow 4d^{10}6d\ ^2D_{3/2}$ .

**Table 1.** Possible resonant photo-ionization schemes of silver; ground state configuration of Ag is  $4d^{10}5s\ ^2S_{1/2}$ .

First Transition $\lambda$ (nm)	First Excited Level (Term; J)	Second Transition $\lambda$ (nm)	Second Excited Level (Term; J)
<u>328.163</u>	<u><math>4d^{10}5p\ (^2P^o; 3/2)</math></u>	362.514	$4d^{10}8d\ (^2D; 5/2)$
		371.026	$4d^{10}9s\ (^2S; 1/2)$
		381.205	$4d^{10}7d\ (^2D; 5/2)$
		<u>421.402</u>	<u><math>4d^{10}6d\ (^2D; 3/2)</math></u>
		466.983	$4d^{10}7s\ (^2S; 1/2)$
		546.707	$4d^{10}5d\ (^2D; 5/2)$
338.387	$4d^{10}5p\ (^2P^o; 1/2)$	368.357	$4d^{10}7d\ (^2D; 3/2)$
		384.186	$4d^{10}8s\ (^2S; 1/2)$
		405.666	$4d^{10}6d\ (^2D; 3/2)$
		447.734	$4d^{10}7s\ (^2S; 1/2)$
		521.059	$4d^{10}5d\ (^2D; 3/2)$

## 2.2. Doppler Broadening

Moving atoms experience a Doppler shift of the incident laser radiation. The shifted frequency is given by:

$$\nu = \nu_0(1 \pm \frac{v}{c}) \quad (1)$$

where  $\nu_0$  is the initial frequency,  $v$  is the velocity of the atoms along the laser beam and  $c$  is the speed of light.

In this experiment, the environment is an ablation plume where there is a very wide velocity distribution attributed to the high temperature of the plume. This contributes to a large Doppler broadening in terms of GHz for each transition line, which is a limiting factor to the resolution of spectroscopic investigations in hot environments.

In the individual frames of reference of the excitation lasers, the atoms in the trajectory of each excitation laser experience a Doppler effect with respect to the atomic transition lines. When the Doppler-shifted resonant frequencies of these atoms match the frequency of the excitation laser, the atoms will be resonantly excited. In this state, if the complementary excitation laser is tuned at a frequency with the corresponding shift, or has a linewidth sufficient to cover the corresponding shift from its central frequency, subsequent transitions occur and resonant photo-ionization can be achieved over these ranges of frequency values.

## 2.3. Best Fit of Experimental Resonance Profiles

When an atomic line is scanned with a laser having a linewidth larger than that of the atomic line, the laser profile is effectively reproduced in the resonance profile. In a scenario where Doppler broadening is present, the resonance profile becomes wider with additional Gaussian contribution.

Centered Lorentzian distribution  $L(x;\gamma)$  and Gaussian distribution  $G(x;\sigma)$  with profile parameters  $\gamma$  and  $\sigma$ , respectively, are given by

$$L(x;\gamma) = \frac{\gamma}{\pi(x^2 + \gamma^2)} \quad (2)$$

$$G(x;\sigma) = \frac{e^{-x^2/2\sigma^2}}{\sigma\sqrt{2\pi}} \quad (3)$$

Full width at half maximum (FWHM) of a Lorentzian profile is  $f_L = 2\gamma$  and of a Gaussian profile is  $f_G \approx 2.355\sigma$ .

The Voigt profile is a probability distribution given by a convolution of a Lorentzian distribution and a Gaussian distribution. It is often used in analyzing data from spectroscopy where different contributions to the line profiles are present.

$$V(x; \sigma, \gamma) = \int_{-\infty}^{\infty} G(x'; \sigma) L(x - x'; \gamma) dx' \quad (4)$$

where  $x'$  is the shift from the line center.

The FWHM of a Voigt profile can be calculated to an accuracy of 0.02% using the following relation [21]:

$$f_V \approx 0.5346f_L + \sqrt{0.2166f_L^2 + f_G^2} \quad (5)$$

The  $\gamma$  and  $\sigma$  fit parameters are reported for different resonance profiles with the corresponding fit curves in Section 4. The resulting peak amplitude and the FWHM values of the fitted profiles are derived with a high level of confidence and a relative error of less than 7%, mainly due to the noisy character of the data.

### 3. Materials and Methods

Figure 2 shows a schematic sketch of the experimental apparatus that is described in detail in the following sub-sections.

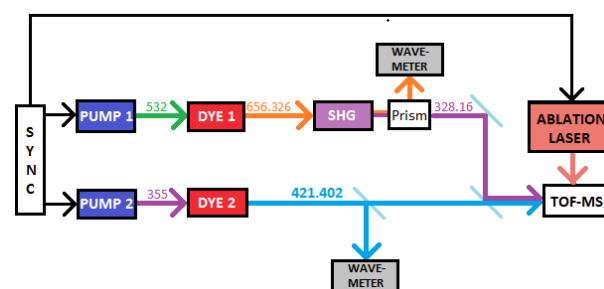


**Figure 2.** Experimental set-up for the laser photoionization study of Ag. PUMP 1 and PUMP 2 represent the pump Nd:YAG lasers, while DYE 1 and DYE 2 represent the dye lasers, respectively. SHG is the second harmonic generation crystal and TOF-MS represents the time-of-flight mass spectrometer.

#### 3.1. Dye Laser Systems

Both the transitional wavelengths were generated using dye lasers. The first step was provided by a Quantel TDL50 dye laser pumped with a 532 nm (1.1 W @ 10 Hz) beam from a Quantel YG 580 laser. The dye solution used was sulforhodamine 640 (0.3 g/L for the oscillator and 0.075 g/L for the amplifier) with methanol solvent [22]. This dye laser was tuned at 656.326 nm; then, the resulting laser beam was frequency doubled with a second harmonic generation (SHG) crystal, which produced UV light at 328.163 nm. After the frequency doubling, the fundamental (656.326 nm) and the second harmonic (328.163 nm) were spatially separated by passing through a prism. The fundamental beam was sent to a HighFinesse WS7 wavemeter to continuously monitor the wavelength.

The second step was provided by a Lambda Physik FL2002 dye laser pumped with 355 nm (0.5 W @ 10 Hz) from a Quantel YG 980. The dye solution used was Stilbene 420 (0.25 g/L both for the oscillator and the pre-amplifier) with methanol solvent [22]. The system was tuned at 421.402 nm. The two pump lasers and the ablation laser were synchronized and it was possible, therefore, to experimentally optimize the time delay between the laser pulses.

### 3.2. TOF-MS

In Figure 2, TOF-MS stands for time-of-flight mass spectrometer, which was set up in the SPES off-line laser laboratory, as discussed in [13]. The system was maintained at high vacuum in the range of  $10^{-7}$  mbar and had a flight length of 1.90 m, with a micro-channel plate (MCP) detector for the collection of the ions. The TOF-MS was coupled with an Nd:YAG ablation laser (1064 nm), which was directed onto a solid target and placed inside the TOF-MS housing to create a vapor of atoms. The excitation lasers were sent into the ablation plume and the ions, created as a consequence of photo-ionization in the interaction volume, were directed towards the MCP with the finely tuned ion-optics system, as shown in Figure 3.

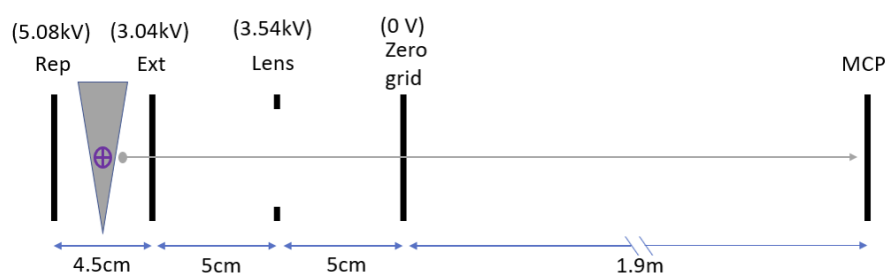


**Figure 3.** A schematic representation of the ion-optics inside the TOF-MS. The four electrodes indicated are: a repeller plate (Rep), an extraction grid (Ext), an electrostatic lens and a zero-voltage grid. The grey triangle (not to scale) represents an upward-expanding conical plume of silver and the purple cross-mark indicates the excitation lasers incidence orthogonal to the vertical axis of the plume. The grey dot represents a laser-ionized silver ion which is guided to the MCP with the ion-optics system.

### 3.3. Target and Ablation Technique

The disc-shaped silver targets (5 mm in diameter, 1 mm thick) were purchased from *Carlo Erba Reagents S.r.l.*. The target was 99.9% pure silver composed of 51.83% natural abundance ( $^{107}\text{Ag}$ ) and 48.17% ( $^{109}\text{Ag}$ ).

The ablation laser was a Quantel YG 980 capable of 20 ns pulses up to 2 J energy at a 1064 nm @10 Hz repetition rate. The ablation pulse was fired on a silver target 30–35  $\mu\text{s}$  before the first excitation laser. A weakly focused ablation beam was focused incident on the surface of the solid target. The beam was focused just sufficiently to cover the surface area of the solid silver target. The power of the ablation laser used was 0.8–0.9 W, with a spot-size of  $\sim 4.9$  mm (power density  $\sim 4.2$ – $4.7$  W/cm $^2$ ) on the target surface. The resulting plume was nearly conical with a vertical central axis. The low ablation laser energy level was set in order to generate atom ablation while avoiding the generation of an ionized plasma with potential damage to the MCP.

## 4. Experimental Conditions and Results

The data acquisition, the readings of the lambda-meter and the automatic wavelength scan of the excitation lasers TDL50 and FL2002 were operated through a Matlab program.

### 4.1. Isotopic Identification

Figure 4 shows a TOF signal of silver as collected on the MCP. As can be seen, the two isotopes  $^{107}\text{Ag}$  and  $^{109}\text{Ag}$  were detected separately with a satisfying time resolution. In the configuration of the ion-optics described in Section 3.2,  $^{107}\text{Ag}$  and  $^{109}\text{Ag}$  arrived at the MCP at 2.672  $\mu\text{s}$  and 2.698  $\mu\text{s}$ , respectively.

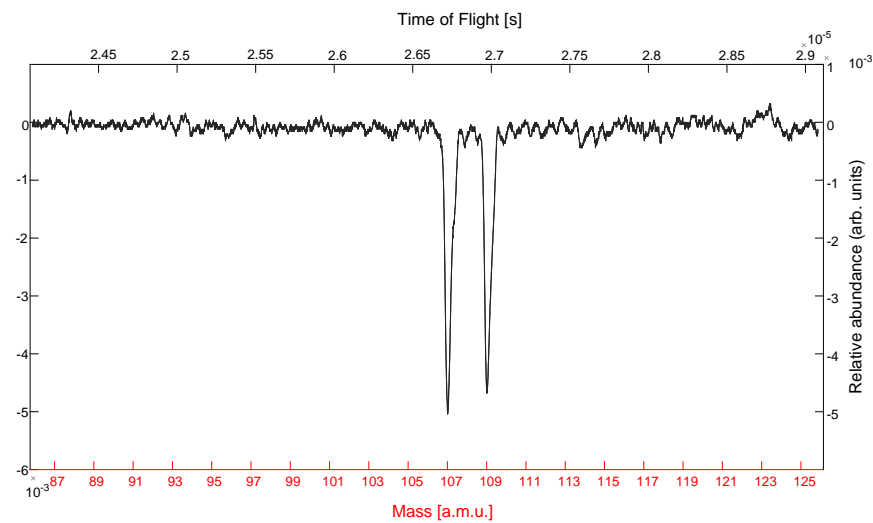


**Figure 4.** Detected TOF signal of Ag. The signal is plotted against time (upper x-axis) and against mass (lower x-axis).

#### 4.2. Doppler-Suppressed Scheme Test: $4d^{10}5s\ 2S_{1/2} \rightarrow 4d^{10}5p\ 2P_{3/2}^o \rightarrow 4d^{10}6d\ 2D_{3/2}$

The key to avoiding Doppler broadening is to avoid different velocity components in the given environment. The approach used to avoid this broadening was to probe only a tiny volume inside the plume, largely containing only single velocity components.

Both the excitation lasers were directed into the ablation plume in the plane orthogonal to the vertical central axis of the plume. This implies that the Doppler effect was confined with just the horizontal components of the atomic velocities. If the excitation lasers are injected non-collinearly to each other, this will reduce the volume of the interaction region by a large factor compared to collinear injection. Smaller diameters of the laser beams provide a smaller interaction volume and are essential for selecting a group of atoms with almost zero horizontal velocity close to the central axis of the plume. Higher angular separation of the excitation lasers ensures this selection even further.

The diameters of the laser beams used to attain the desired interaction volume were 0.6–0.8 mm and 1.0–1.2 mm for the first and second step transition lasers, respectively. These laser beams were maintained at an angular separation of  $\sim 8.5$  degrees and, in this configuration, a very small intersection volume,  $\sim 0.5\text{ mm}^3$ , was achieved inside the ablation plume. This precise selection of the interaction volume enabled us to produce a nearly Doppler-suppressed scan of the transition lines in the ablation plume.

Figures 5 and 6 show clear resonance of the first step and the second step at 328.163 nm and 421.402 nm, respectively. The resonance profiles reflect very narrow linewidths of  $\sim 1.2\text{ pm}$  (3.3 GHz) and  $\sim 1.0\text{ pm}$  (1.7 GHz). The respective laser profiles, with corresponding linewidths, were reproduced (see Table 2), showing practically no effect of Doppler broadening.

**Table 2.** Parameters of the excitation lasers.

Laser	Fundamental			$\lambda$	SHG		Power ( $\mu\text{W}$ )	Pulse Length (ns)
	$\lambda$ (nm)	$\Delta\lambda$ (pm)	$\Delta\nu$ (GHz)		$\Delta\lambda$ (pm)	$\Delta\nu$ (GHz)		
TDL50	656.326	3–3.5	2.1–2.4	328.163	1.1–1.2	3.0–3.3	20–30	20
FL2002	421.402	1–1.1	1.7–1.9	-	-	-	500–550	20

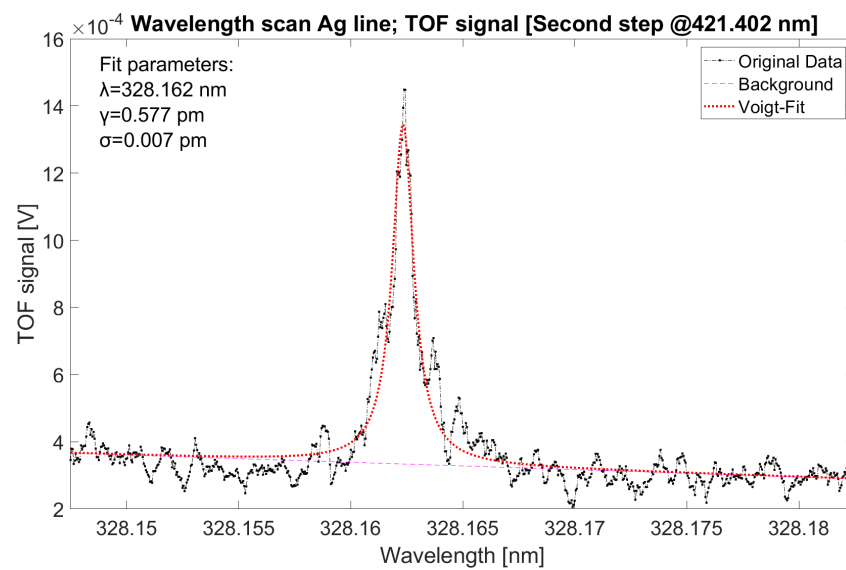


**Figure 5.** First transition step wavelength scan  $4d^{10}5s^2S_{1/2} \rightarrow 4d^{10}5p^2P_{3/2}^o$  Scanning range = 28 pm (77.9 GHz).

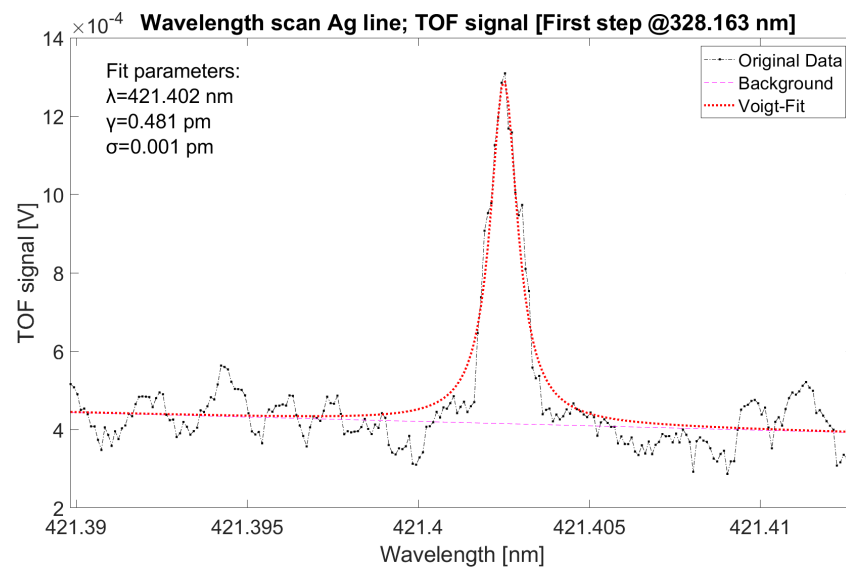


**Figure 6.** Second transition step wavelength scan  $4d^{10}5p^2P_{3/2}^o \rightarrow 4d^{10}6d^2D_{3/2}$  Scanning range = 22 pm (37.2 GHz).

#### 4.3. Effect of Laser Linewidth on Doppler Broadening

For the next part of the experiment, an effort was made to study the Doppler-affected scenario and the effect of the linewidths of the excitation laser lights.

The experimental condition changes for these scans were: (a) nearly collinear injection of the excitation lasers and, (b) larger beam diameter of the first step laser, increased to 1–1.5 mm. These changes enabled us to work with a larger interaction volume which contained a higher velocity distribution, resulting in Doppler broadening.

Figure 7 shows a wavelength scan of the first transition step affected by Doppler broadening. As can be seen, the Gaussian contribution increased to 0.861 pm compared to 0.007 pm in the Doppler-free case shown in Figure 5, thereby increasing the linewidth of the resonance profile to  $\sim 2.7$  pm (7.5 GHz) from  $\sim 1.2$  pm (3.3 GHz). This is the frequency range within which  $Ag^+$  ions can be produced using the laser wavelengths with the given linewidths (see Table 2).



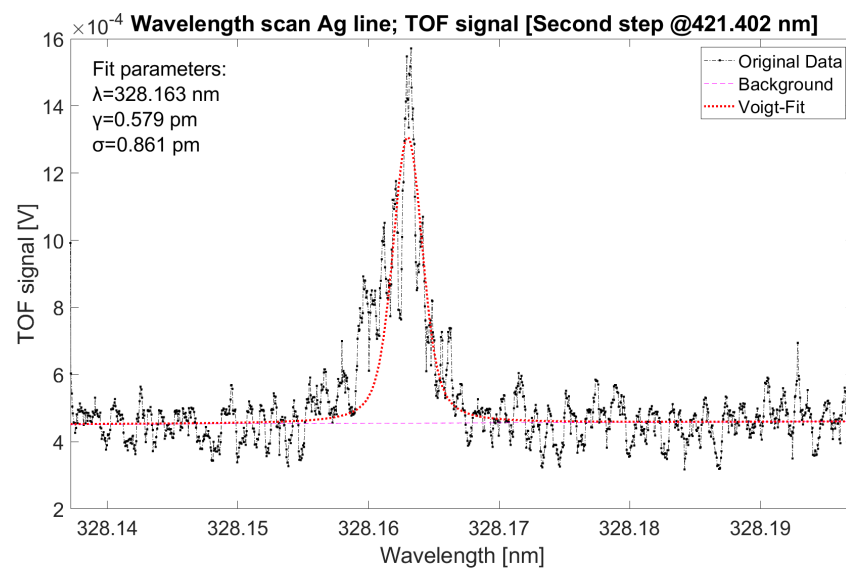


**Figure 7.** First-step Doppler broadening; scanned with second-step laser operating as single-mode laser @421.402 nm Scanning range = 68 pm (189.3 GHz).

Using lasers of narrow linewidths for ion production entails the disadvantage of losing many atoms which are affected by the Doppler effect. To avoid this loss, lasers of large linewidths are used for ion production in laser ion sources (LIS).

To study this scenario, the pumping power in the dye oscillator of the second dye laser was increased to push the gain of the cavity far beyond the gain threshold, thereby allowing additional modes to resonate effectively in the oscillator cavity. The pumping power was increased to such a level that, not only the extra modes were created in the oscillator cavity, but these modes were power-broadened to form a nearly continuous broad laser profile with an effective linewidth of  $\sim 10$ – $15$  pm, corresponding to  $\sim 16.9$ – $25.3$  GHz. At this stage, the amplification of the laser beam exiting from the oscillator cavity was reduced to maintain similar power to the central mode by carefully monitoring the intensity of the ion signal. This procedure was performed to emphasize the effect of the spectral linewidth of the excitation laser light. The overall laser power of the second dye laser in this configuration was 850–900  $\mu$ W.

Figure 8 shows the resonance profile of the first-step wavelength scan with the second-step laser kept in multi-mode. The linewidth of the profile showed a significant increase to  $\sim 7.5$  pm, corresponding to  $\sim 20.9$  GHz. Compared to Figure 7, the area under the curve increased by  $\sim 3.5$  times, indicating proportional change in the number of ions collected. In other words, if the first-step laser had a linewidth of around 20.9 GHz, it would produce a similar amount of ions by just being maintained at the resonant wavelength, 328.163 nm. This represents clear qualitative confirmation that broad linewidth of the excitation lasers can produce higher ion production in a hot environment where the Doppler effect is dominantly present.

Using lasers of linewidth around 10 GHz is quite common for the purpose of ion production in laser ion sources to capture Doppler-shifted atoms and to ensure higher ion production. However, the use of a much larger linewidth increases the chance of probing other nearby atomic lines of other elements, which could compromise the chemical selectivity of the laser ion source.



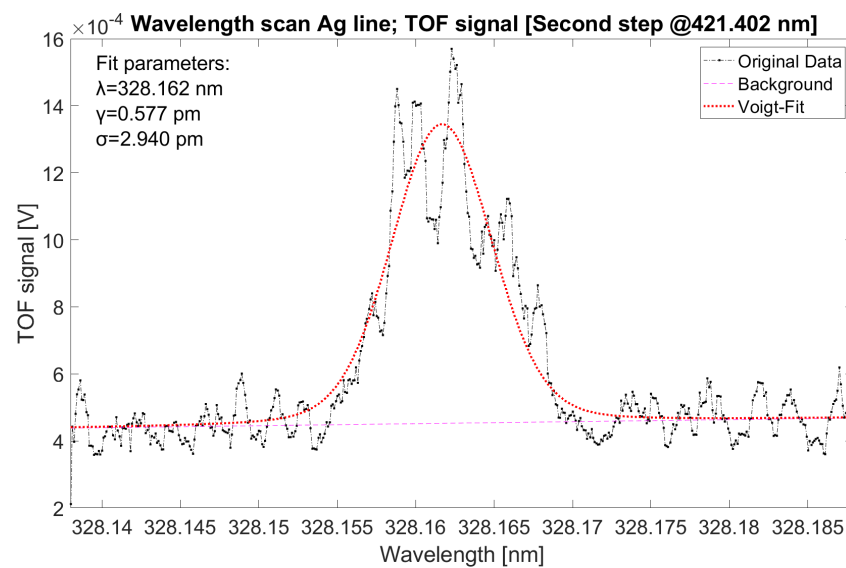


**Figure 8.** First-step Doppler broadening; scanned with second-step laser, operating as a multi-mode laser with central frequency @421.402 nm Scanning range = 50 pm (139.2 GHz).

#### 4.4. Fine Structures of the Level $4d^{10}6d^2D$ ( $J = 5/2$ and $J = 3/2$ )

Figure 9 shows clearly the fine structure split of the Ag-level  $4d^{10}6d^2D$ . The scan shows resonance peaks at 421.217 nm and 421.402 nm, corresponding to the transitions to  $J = 5/2$  (left) and  $J = 3/2$  (right), respectively. The fine structures show a split of roughly  $186 \pm 2$  pm, corresponding to  $314 \pm 3$  GHz, in accordance with the National Institute of Standards and Technology (NIST) database value of 185 pm, corresponding to 312.5 GHz [17].

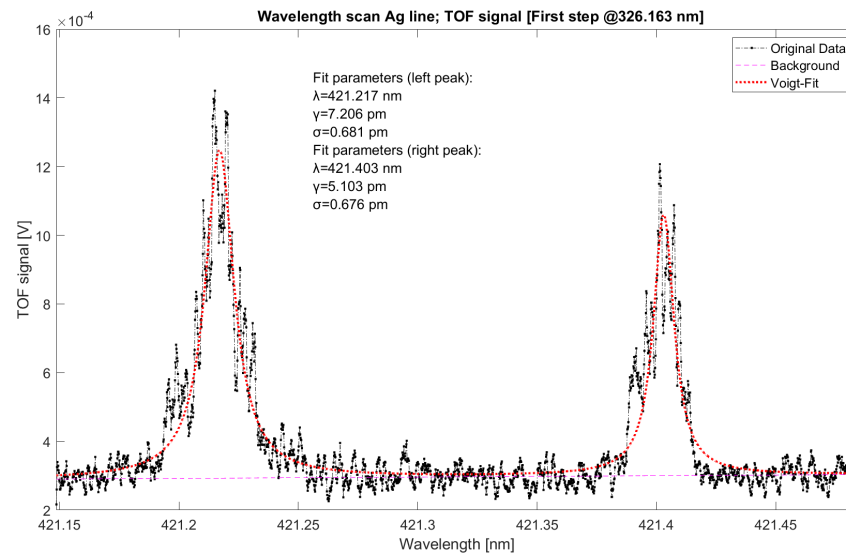


**Figure 9.** Fine structure of  $4d^{10}6d^2D$  [ $J = 5/2$  (left peak) and  $J = 3/2$  (right peak)]. Scanning range = 330 pm (557.4 GHz).

Qualitatively, the left peak had a higher intensity and could indicate higher transitional probability of the line. According to this measurement, the second-step transition to  $J = 5/2$  would be the preferred choice for production of  $\text{Ag}^+$  ions in the SPES facility. Quantitative comparison of the relative intensity of the two transitions can, unfortunately, not be provided as the stability of the ablation plume intensity was not determined sufficiently precisely.

## 5. Conclusions

In this study, two-step resonant photoionization schemes for Ag were implemented and will be used for on-line production of  $\text{Ag}^+$  ions in the SPES project. Doppler-free spectroscopy of these Ag lines was successfully performed in an ablation plume. Doppler broadening with collinear injection of the excitation lasers and effects of the linewidths of the excitation lasers were thoroughly demonstrated. The fine structure of the Ag level  $4d^{10}6d^2D$  was verified, with a split of  $314 \pm 3$  GHz, thus providing two possible pathways for the laser photo-ionization of Ag.

**Author Contributions:** Conceptualization, O.S.K., E.M. and D.S.; methodology, O.S.K.; software, O.S.K. and D.S.; validation, O.S.K., E.M., D.S. and P.N.; formal analysis, O.S.K. and A.A. (Alberto Arzenton); investigation, O.S.K.; resources, E.M. and D.S.; data curation, O.S.K., E.M., D.S., A.K., P.N., S.F. and A.A. (Alberto Arzenton); writing—original draft preparation, O.S.K., E.M., D.S. and P.N.; writing—review and editing, O.S.K., E.M., D.S. and P.N.; visualization, O.S.K.; supervision, E.M. and D.S.; project administration, A.A. (Alberto Andrighetto) All authors have read and agreed to the published version of the manuscript.

**Funding:** This research received no external funding.

**Data Availability Statement:** The data that support the findings of this study are available from the corresponding author upon reasonable request.

**Acknowledgments:** We thank the SPES and the ISOLPHARM collaboration for all the support provided.

**Conflicts of Interest:** The authors declare no conflict of interest.

## Abbreviations

The following abbreviations are used in this manuscript:

SPES	Selective Production of Exotic Species
RILIS	Resonant ionization laser ion source
RIB	Radioactive ion beam
ISOL	Isotope separation on-line
LNL	Legnaro National Laboratories
UC	Uranium carbide
Ti-Sa	Titanium sapphire
TOF-MS	Time-of-flight mass spectrometer
IP	Ionization potential
FWHM	Full width at half maximum
SHG	Second harmonic generation
MCP	Micro-channel plate
NIST	National Institute of Standards and Technology
LIS	Laser ion source

## References

1. Alkhazov, G.D.; Batist, L.K.; Bykov, A.A.; Vitman, V.D.; Letokhov, V.S.; Mishin, V.I.; Panteleyev, V.N.; Sekatsky, S.K.; Fedoseyev, V.N. Application of a high efficiency selective laser ion source at the IRIS facility. *Nucl. Instrum. Methods Phys. Res. A* **1991**, *306*, 400–402. [\[CrossRef\]](#)
2. Rothe, S.; Goodacre, T.D.; Fedorov, D.V.; Fedosseev, V.N.; Marsh, B.A.; Molkanov, P.L.; Rossel, R.E.; Seliverstov, M.D.; Veinhard, M.; Wendt, K.D.A. Laser ion beam production at CERN-ISOLDE: New features—More possibilities. *Nucl. Instrum. Methods Phys. Res. B* **2016**, *376*, 91–96. [\[CrossRef\]](#)
3. Fedosseev, V.N.; Kudryavtsev, Y.; Mishin, V.I. Resonance laser ionization of atoms for nuclear physics. *Phys. Scr.* **2012**, *85*, 058104. [\[CrossRef\]](#)
4. Lassen, J.; Bricault, P.; Dombbsky, M.; Lavoie, J.P.; Geppert, C.; Wendt, K. Resonant Ionization Laser Ion Source Project at TRIUMF. In *Laser 2004*; Błaszczyk, Z., Markov, B., Marinova, K., Eds.; Springer: Berlin/Heidelberg, Germany, 2004. [\[CrossRef\]](#)
5. Lecesne, N.; Alves-Conde, R.; Coterreanu, E.; De Oliveira, F.; Dubois, M.; Flambard, J.L.; Franberg, H.; Gottwald, T.; Jardin, P.; Lassen, J.; et al. GISELE: A resonant ionization laser ion source for the production of radioactive ions at GANIL. *Rev. Sci. Instrum.* **2010**, *81*, 02A910. [\[CrossRef\]](#) [\[PubMed\]](#)

6. Ewald, G.; Nörtershäuser, W.; Dax, A.; Götze, S.; Kirchner, R.; Kluge, H.-J.; Kühl, T.; Sanchez, R.; Wojtaszek, A.; Bushaw, B. Nuclear Charge Radii of Li8,9 Determined by Laser Spectroscopy. *Phys. Rev. Lett.* **2004**, *93*, 113002. [CrossRef] [PubMed]
7. Sonoda, T.; Iimura, H.; Reponen, M.; Wada, M.; Katayama, I.; Sonnenschein, V.; Takamatsu, T.; Tomita, H.; Kojima, T.M. The laser and optical system for the RIBF-PALIS experiment. *Nuclear Inst. Methods Phys. Res. A* **2018**, *877*, 118–123. [CrossRef]
8. Moore, I.D.; Nieminen, A.; Billowes, J.; Campbell, P.; Geppert, C.; Jokinen, A.; Kessler, T.; Marsh, B.; Penttilä, H.; Rinta-Antila, S.; et al. Development of a laser ion source at IGISOL. *J. Phys. G Nucl. Part. Phys.* **2005**, *31*, S1499. [CrossRef]
9. Kudryavtsev, Y.A.; Andrzejewski, J.; Bijmens, N.; Franchoo, S.; Huyse, M.; Piechaczek, A.; Szerypo, J.; Reusen, I.; Van Duppen, P.; Vermeeren, L.; et al. Laser ion source for the Leuven Isotope Separator on-line. *Rev. Sci. Instrum.* **1996**, *67*, 938. [CrossRef]
10. Grüning, C.; Huber, G.; Klopp, P.; Kratz, J.V.; Kunz, P.; Passler, G.; Trautmann, N.; Waldek, A.; Wendt, K. Resonance ionization mass spectrometry for ultratrace analysis of plutonium with a new solid state laser system. *Int. J. Mass Spectrom.* **2004**, *235*, 171–178. [CrossRef]
11. Scarpa, D.; Mariotti, E.; Khwairakpam, O.S.; Parenti, V.; Buono, A.; Nicolosi, P.; Calderolla, M.; Khanbekyan, A.; Ballan, M.; Centofante, L.; et al. New solid state laser system for SPES: Selective Production of Exotic Species project at Laboratori Nazionali di Legnaro. *Rev. Sci. Instrum.* **2022**, *93*, 083001. [CrossRef] [PubMed]
12. Scarpa, D.; Barzakh, A.; Fedorov, D.; Andrighetto, A.; Mariotti, E.; Nicolosi, P.; Tomaselli, A. First results on Ge resonant laser photoionization in hollow cathode lamp. *Rev. Sci. Instrum.* **2016**, *87*, 02B708. [CrossRef] [PubMed]
13. Scarpa, D.; Fedorov, D.; Andrighetto, A.; Mariotti, E.; Nicolosi, P.; Sottili, L.; Tomaselli, A.; Cecchi, R.; Stiaccini, L. ToF diagnostic of Tin resonant laser photoionization in SPES laser off-line laboratory. *JINST* **2016**, *11*, C09001. [CrossRef]
14. Scarpa, D.; Makhathini, L.; Tomaselli, A.; Grassi, D.; Corradetti, S.; Manzolaro, M.; Vasquez, J.; Calderolla, M.; Rossignoli, M.; Monetti, A.; et al. Photo-ionization of aluminum in a hot cavity for the selective production of exotic species project. *Rev. Sci. Instrum.* **2014**, *85*, 02B908. [CrossRef] [PubMed]
15. Jading Y.; Catherall, R.; Fedoseyev, V.N.; Jokinen, A.; Jonsson, O.C.; Kautzsch, T.; Klockl, I.; Kratz, K.L.; Kugler, E.; Lettry, J.; et al. Production of radioactive Ag ion beams with a chemically selective laser ion source. *Nucl. Instr. Meth. Phys. Res. B* **1997**, *126*, 76–80. [CrossRef]
16. Andrighetto, A.; Tosato, M.; Ballan, M.; Corradetti, S.; Borgna, F.; Di Marco, V.; Marzaro, G.; Realdon, N. The ISOLPHARM project: ISOL-based production of radionuclides for medical applications. *J. Radioanal. Nucl. Chem.* **2019**, *322*, 73–77. [CrossRef]
17. NIST. Available on-line: <https://physics.nist.gov/PhysRefData/ASD/> (accessed on 28 October 2022).
18. Reponen, M.; Kessler, T.; Moore, I.D.; Rothe, S.; Äystö, J. A hot cavity laser ion source at IGISOL. *Eur. Phys. J. A* **2009**, *42*, 509. [CrossRef]
19. Geppert, C. Laser systems for on-line laser ion sources. *Nucl. Instrum. Methods Phys. Res. B Beam Interact. Mater. Atoms* **2008**, *266*, 4354–4361. [CrossRef]
20. Fedoseyev, V.N.; Jading, Y.; Jonsson, O.C.; Kirchner, R.; Kratz, K.L.; Krieg, M.; Kugler, E.; Lettry, J.; Mehren, T.; Mishin, V.I.; et al. Study of short-lived silver isotopes with a laser ion source. *Z. Phys. A—Hadron. Nucl.* **1995**, *353*, 9–10. [CrossRef]
21. Olivero, J.J.; Longbothum, R.L. Empirical fits to the Voigt line width: A brief review. *J. Quant. Spectrosc. Radiat. Transf.* **1977**, *17*, 233–236. [CrossRef]
22. Brackmann, U. *Lambdachrome® Laser Dyes*; Lambda Physik GmbH: Goettingen, Germany, 2000; pp. 83, 191.

**Disclaimer/Publisher’s Note:** The statements, opinions and data contained in all publications are solely those of the individual author(s) and contributor(s) and not of MDPI and/or the editor(s). MDPI and/or the editor(s) disclaim responsibility for any injury to people or property resulting from any ideas, methods, instructions or products referred to in the content.